

# Room temperature continuous wave operation of InAs/GaAs quantum dot photonic crystal nanocavity laser on silicon substrate

Katsuaki Tanabe, Masahiro Nomura, Denis Guimard,  
Satoshi Iwamoto, and Yasuhiko Arakawa

*Institute for Nano Quantum Information Electronics, Research Center for Advanced Science and Technology, and  
Institute of Industrial Science, University of Tokyo, Tokyo 153-8505, Japan*  
[tanabe@iis.u-tokyo.ac.jp](mailto:tanabe@iis.u-tokyo.ac.jp)

**Abstract:** Room temperature, continuous-wave lasing in a quantum dot photonic crystal nanocavity on a Si substrate has been demonstrated by optical pumping. The laser was an air-bridge structure of a two-dimensional photonic crystal GaAs slab with InAs quantum dots inside on a Si substrate fabricated through wafer bonding and layer transfer. This surface-emitting laser exhibited emission at 1.3  $\mu\text{m}$  with a threshold absorbed power of 2  $\mu\text{W}$ , the lowest out of any type of lasers on silicon.

© 2009 Optical Society of America

**OCIS codes:** (130.3990) Micro-optical devices; (230.5298) Photonic crystals; (250.5300) Photonic integrated circuits; (230.5590) Quantum-well, -wire, and -dot devices; (250.5960) Semiconductor lasers

---

## References and links

1. H. Park, A. W. Fang, S. Kodama, and J. E. Bowers, "Hybrid silicon evanescent laser fabricated with a silicon waveguide and III-V offset quantum wells," *Opt. Express* **13**, 9460-9464 (2005).
2. A. W. Fang, R. Jones, H. Park, O. Cohen, O. Raday, M. J. Paniccia, and J. E. Bowers, "Integrated AlGaInAs-silicon evanescent racetrack laser and photodetector," *Opt. Express* **15**, 2315-2322 (2007).
3. C. Monat, C. Seassal, X. Letartre, P. Viktorovitch, P. Regreny, M. Gendry, P. Rojo-Romeo, G. Hollinger, E. Jalaguier, S. Pocas, and B. Aspar, "InP 2D photonic crystal microlasers on silicon wafer: room temperature operation at 1.55  $\mu\text{m}$ ," *Electron. Lett.* **37**, 764-766 (2001).
4. C. Monat, C. Seassal, X. Letartre, R. Regreny, P. Rojo-Romeo, P. Viktorovitch, M. L. d'Yerville, D. Cassagne, J. P. Albert, E. Jalaguier, S. Pocas, and B. Aspar, "InP-based two-dimensional photonic crystal on silicon: In-plane Bloch mode laser," *Appl. Phys. Lett.* **81**, 5102-5104 (2002).
5. J. Mouette, C. Seassal, X. Letartre, P. Rojo-Romeo, J. Leclereq, P. Regreny, P. Viktorovitch, E. Jalaguier, P. Perreau, and H. Moriceau, "Very low threshold vertical emitting laser operation in InP graphite photonic crystal slab on silicon," *Electron. Lett.* **39**, 526-528 (2003).
6. G. Vecchi, F. Raineri, I. Sagnes, A. Yacomotti, P. Monnier, T. J. Karle, K. Lee, R. Bravive, L. L. Gratiot, S. Guilet, G. Beaudoin, A. Talneau, S. Bouchoule, A. Levenson, and R. Raj, "Continuous-wave operation of photonic band-edge laser near 1.55  $\mu\text{m}$  on silicon wafer," *Opt. Express* **15**, 7551-7556 (2007).
7. C. Monat, C. Seassal, X. Letartre, P. Regreny, P. Rojo-Romeo, P. Viktorovitch, M. Le Vassor d'Yerville, D. Cassagne, J. P. Albert, E. Jalaguier, S. Pocas, and B. Aspar, "Modal analysis and engineering on InP-based two-dimensional photonic-crystal microlasers on a Si wafer," *IEEE J. Quantum Electron.* **39**, 419-425 (2003).
8. M. H. Shih, A. Mock, M. Bagheri, N. Suh, S. Farrell, S. Choi, J. D. O'Brien, and P. D. Dapkus, "Photonic crystal lasers in InGaAsP on a SiO<sub>2</sub>/Si substrate and its thermal impedance," *Opt. Express* **15**, 227-232 (2007).
9. Y. Arakawa and H. Sakaki, "Multidimensional quantum well laser and temperature dependence of its threshold current," *Appl. Phys. Lett.* **40**, 939-941 (1982).
10. P. Bhattacharya and Z. Mi, "Quantum-dot optoelectronic devices," *Proc. IEEE* **95**, 1723-1740 (2007).
11. T. Yoshie, O. B. Shchekin, H. Chen, D. G. Deppe, and A. Scherer, "Quantum dot photonic crystal lasers," *Electron. Lett.* **38**, 967-968 (2002).
12. M. Nomura, S. Iwamoto, K. Watanabe, N. Kumagai, Y. Nakata, S. Ishida, and Y. Arakawa, "Room temperature continuous-wave lasing in photonic crystal nanocavity," *Opt. Express* **14**, 6308-6315 (2006).
13. M. Nomura, S. Iwamoto, N. Kumagai, and Y. Arakawa, "Temporal coherence of a photonic crystal nanocavity laser with high spontaneous emission coupling factor," *Phys. Rev. B* **75**, 195313 (2007).
14. B. Ben Bakir, C. Seassal, X. Letartre, P. Regreny, M. Gendry, P. Viktorovitch, M. Zussy, L. Di Cioccio, and J. M. Fedeli, "Room-temperature InAs/InP quantum dots laser operation based on heterogeneous "2.5 D" Photonic Crystal," *Opt. Express* **14**, 9269-9276 (2006).

15. X. Letartre, C. Monat, C. Seassal, and P. Viktorovitch, "Analytical modeling and an experimental investigation of two-dimensional photonic crystal microlasers: defect state (microcavity) versus band-edge state (distributed feedback) structures," *J. Opt. Soc. Am. B* **22**, 2581-2595 (2005).
16. M. Nomura, S. Iwamoto, A. Tandaechanurat, Y. Ota, N. Kumagai, and Y. Arakawa, "Photonic band-edge micro lasers with quantum dot gain," *Opt. Express* **17**, 640-648 (2009).
17. D. Guimard, M. Nishioka, S. Tsukamoto, and Y. Arakawa, "High density InAs/GaAs quantum dots with enhanced photoluminescence intensity using antimony-mediated metal organic chemical vapor deposition," *Appl. Phys. Lett.* **89**, 183124 (2006).
18. D. Guimard, M. Ishida, L. Li, M. Nishioka, Y. Tanaka, H. Sudo, T. Yamamoto, H. Kondo, M. Sugawara, and Y. Arakawa, "Interface properties of InAs quantum dots produced by antimony surfactant-mediated growth: etching of segregated antimony and its impact on the photoluminescence and lasing characteristics," *Appl. Phys. Lett.* **94**, 103116 (2009).
19. K. Tanabe, A. Fontcuberta i Morral, H. A. Atwater, D. J. Aiken, and M. W. Wanlass, "Direct-bonded GaAs/InGaAs tandem solar cell," *Appl. Phys. Lett.* **89**, 102106 (2006).
20. Y. Mori and N. Watanabe, "A new etching solution system,  $H_3PO_4-H_2O_2-H_2O$ , for GaAs and its kinetics," *J. Electrochem. Soc.* **125**, 1510-1514 (1978).
21. G. C. DeSalvo, W. F. Tseng, and J. Comas, "Etch rates and selectivities of citric acid/hydrogen peroxide on GaAs,  $Al_{0.3}Ga_{0.7}As$ ,  $In_{0.2}Ga_{0.8}As$ ,  $In_{0.53}Ga_{0.47}As$ ,  $In_{0.52}Al_{0.48}As$ , and InP," *J. Electrochem. Soc.* **139**, 831-835 (1992).
22. C. Carter-Coman, R. Bicknell-Tassius, R. G. Benz, A. S. Brown, and N. M. Jokerst, "Analysis of GaAs substrate removal etching with citric acid: $H_2O_2$  and  $NH_4OH:H_2O_2$  for application to compliant substrates," *J. Electrochem. Soc.* **144**, L29-L31 (1997).
23. Y. Akahane, T. Asano, B. Song, and S. Noda, "High-Q photonic nanocavity in a two-dimensional photonic crystal," *Nature* **425**, 944-947 (2003).
24. Y. Tanaka, T. Asano, R. Hatsuta, and S. Noda, "Investigation of point-defect cavity formed in two-dimensional photonic crystal slab with one-sided dielectric cladding," *Appl. Phys. Lett.* **88**, 011112 (2006).
25. C. Monat, C. Seassal, X. Letartre, P. Regreny, M. Gendry, P. Rojo-Romeo, P. Viktorovitch, M. Le Vassor d'Yerville, D. Cassagne, J. P. Albert, E. Jalaguier, S. Pocas, and B. Aspar, "Two-dimensional hexagonal-shaped microcavities formed in a two-dimensional photonic crystal on an InP membrane," *J. Appl. Phys.* **93**, 23-31 (2003).
26. S. Strauf, K. Hennessy, M. T. Rakher, Y. Choi, A. Badolato, L. C. Andreani, E. L. Hu, P. M. Petroff, and D. Bouwmeester, "Self-tuned quantum dot gain in photonic crystal lasers," *Phys. Rev. Lett.* **96**, 127404 (2006).
27. G. Björk, A. Karlsson, and Y. Yamamoto, "On the linewidth of microcavity lasers," *Appl. Phys. Lett.* **60**, 304-306 (1992).
28. G. Björk, A. Karlsson, and Y. Yamamoto, "Definition of a laser threshold," *Phys. Rev. A* **50**, 1675-1680 (1994).
29. Y. Ota, M. Nomura, N. Kumagai, K. Watanabe, S. Ishida, S. Iwamoto, and Y. Arakawa, "Enhanced photon emission and absorption of single quantum dot in resonance with two modes in photonic crystal nanocavity," *Appl. Phys. Lett.* **93**, 183114 (2008).

## 1. Introduction

Monolithic devices of III-V semiconductor compound light source or lasers and silicon-based waveguides are promising for integrated optical circuits [1, 2]. Such III-V/Si hybrid devices can compensate the poor ability of silicon as light source due to its low radiative recombination rate stemming from indirect energy bandgaps. Park *et al.* developed a Fabry-Perot laser with a gain medium of AlInGaAs multi quantum wells (MQWs) vertically coupled to a silicon waveguide outlet, paving a way for silicon photonics. Smaller scale, lower threshold lasers built in silicon platforms would bring further benefits for higher integration.

Photonic crystal (PhC) structures can provide wavelength-scale laser cavities with high quality factors ( $Q$ -factors). Spontaneous emission rate to the cavity modes of materials inside small high- $Q$  cavities can be potentially enhanced due to Purcell effect. This enhancement enables low threshold operation of PhC cavity lasers. Monat *et al.* reported the first demonstration of PhC lasers on silicon substrates [3]. A couple of groups presented PhC band edge [4-6] and nanocavity [7, 8] lasers on Si with gain media of In-Ga-As-P system compound MQWs grown on InP substrates layer transferred onto Si substrates using wafer bonding.

Lasers with quantum dot (QD) gain are promising for higher integration with their extremely low lasing threshold, which can minimize thermal accumulation [9]. QD lasers also potentially realize temperature insensitive operation, high output power, large modulation bandwidth and near-zero chirp due to discrete density of states in QDs [10].

Thanks to these advantages, Yoshie *et al.* demonstrated QD-PhC lasers operating at room temperature (RT) with pulsed optical pumping [11]. We previously reported the first demonstration of RT continuous-wave (CW) lasing in QD-PhC nanocavities [12] followed by the lowest lasing threshold absorbed power of 375 nW among any types of lasers at RT [13], both with InAs QDs embedded in GaAs (InAs/GaAs QDs) slabs grown on GaAs substrates.

Ben Bakir *et al.* recently demonstrated an InAs/InP QD-PhC band edge laser transferred onto a Si substrate with a SiO<sub>2</sub>/Si multilayer Bragg reflector inside operating with pulsed pumping at RT [14]. A merit of photonic band-edge or Bloch-mode lasers is potentially higher output power than for PhC cavity-mode or defect-mode lasers [15]. PhC cavity lasers however generally have lower lasing threshold than photonic band-edge lasers do due to the higher in-plane optical confinement and with smaller mode volume of cavities [7, 16]. Other advantages of PhC cavity lasers are represented by the controllability of the *Q*-factor and the mode volumes with the cavity geometry and size to maximize the Purcell factor and thus spontaneous emission rate.

In this paper, we have fabricated InAs/GaAs QD - PhC nanocavity lasers on silicon through wafer bonding and layer transfer techniques and observed their CW lasing at RT by optical pumping. This work is the first demonstration of CW PhC nanocavity lasers on Si operating at RT, to the best of our knowledge, and furthermore the lowest lasing threshold for any type of lasers on silicon reported to date.

## 2. Experimental

### 2.1 Crystal growth of InAs/GaAs quantum dots

A cross-sectional schematic of the laser device-layer structure and fabrication process are shown in Fig. 1. Self-assembled InAs/Sb:GaAs QDs were epitaxially grown by antimony-mediated metal-organic chemical vapor deposition (MOCVD). The use of antimony surfactant allows the growth of high density coalescence-free InAs QDs in the 1.3 μm band with high optical quality [17, 18]. A 300-nm-thick GaAs buffer layer, a 700-nm-thick Al<sub>0.7</sub>Ga<sub>0.3</sub>As etch stop layer and a 220-nm-thick InAs/Sb:GaAs QD slab layer were deposited on a (001) GaAs substrate in this order. The QD slab contained three layers of InAs QDs with a density per layer of  $4 \times 10^{10}$  cm<sup>-2</sup>. The QD layers are separated by 50 nm spacer layers, with the second layer being located at the center of the slab. RT photoluminescence (PL) measurement of the as-grown GaAs-capped InAs QDs showed a peak associated with the ground state emission of the QDs at 1.30 μm with a full width at half maximum (FWHM) of 27 meV.

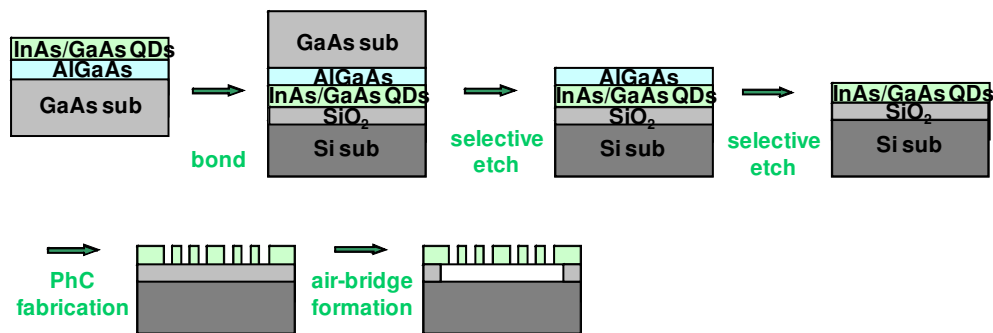


Fig. 1. Cross-sectional schematic of the laser device layer structure and fabrication process.

### 2.2 Layer transfer of InAs/GaAs quantum dot thin films onto SiO<sub>2</sub>/Si substrates

Then the QD slab was transferred onto (001) Si substrates with thermal oxide on top (SiO<sub>2</sub>/Si substrates) through wafer bonding and removal of the GaAs substrate. The SiO<sub>2</sub> thickness was 1 μm, which was estimated through a finite difference time domain (FDTD) calculation to be

large enough to minimize vertical evanescent optical leakage from the QD slab into the Si substrate. The direct wafer bonding and layer transfer techniques adopted in this work are based on previous studies for photovoltaic applications [19]. The GaAs and Si wafers were first coated with photoresist to protect the bonding surfaces from particles generated in the following dicing process because interfacial particles would degrade bonding strength. The wafers were then diced into  $\sim 1 \text{ cm}^2$  area. Then the applied photoresist was removed with acetone along with degreasing of the bonding surfaces. The two wafers were then brought into contact and annealed at  $300 \text{ }^\circ\text{C}$  in atmosphere for 3 hours under uniaxial pressure of 0.1 MPa to promote the formation of covalent bonds between the GaAs and  $\text{SiO}_2$  surfaces. This bonding temperature was adopted to minimize dislocation generation in GaAs caused by strain from thermal expansion mismatch between GaAs and  $\text{SiO}_2/\text{Si}$  while still converting van der Waals bonds formed at RT into covalent Ga-O-Si and As-O-Si bonds. [1, 19]

Then the GaAs substrate was removed by selective chemical etching with  $\text{H}_3\text{PO}_4 - \text{H}_2\text{O}_2$  (3:7 vol.) followed by 50% citric acid -  $\text{H}_2\text{O}_2$  (4:1 vol.) both at RT with the edges of the GaAs wafer coated with photoresist to avoid undercut of the QD slab. The solution compositions were chosen to maximize the etching rate of GaAs for the  $\text{H}_3\text{PO}_4 - \text{H}_2\text{O}_2$  solution [20] and the etching selectivity between GaAs and AlGaAs for the citric acid -  $\text{H}_2\text{O}_2$  solution [21, 22]. The  $\text{Al}_{0.7}\text{Ga}_{0.3}\text{As}$  etch stop layer was then removed by HCl aq. (conc.) at RT.

### 2.3 Fabrication of photonic crystal structures

PhC structures were then formed in the QD slab by forming cylindrical hole arrays through the slab with electron beam lithography and chlorine dry etching. We adopted a point defect structure, called L3 defect, which consists of three missing air holes along the  $\Gamma$ -K direction of the triangular PhC lattice. In addition, the first and third nearest air holes at both edges of the cavity were shifted to outside the cavity to obtain higher cavity  $Q$ -factor [23]. We fabricated a sample with a period of the lattice  $a = 350 \text{ nm}$  and radius of the air hole  $r = 0.27a$ . The first and third nearest air holes at both ends of the cavity were shifted outward by  $0.15a$ . Further design details for this PhC structure are found in Ref. 12.

The  $Q$ -factor for the PhC nanocavities with the  $\text{SiO}_2$  underlayer was as low as  $\sim 1000$  due to the vertical asymmetry causing TE-TM mode coupling loss [24, 25] and not large enough for CW lasing at RT. We therefore removed  $\text{SiO}_2$  under the PhC nanocavities with 20% HF aqueous solution to form air-bridge structures. Despite  $Q$ -factor enhancement, it should be noted that such air-bridge structures have lower thermal dissipation than those sitting on underlayers [25]. Lasing in air-bridge structures therefore could be hindered due to materials degradation caused by excessive thermal accumulation, while the low threshold pump power for our lasers overcome this issue. This semiconductor based air-bridged PhC slab with an air hole array produces an in-plane photonic bandgap. Photons are also confined in the vertical direction due to the refractive index contrast between the slab and air. Figure 2 shows a cross-sectional scanning electron microscope (SEM) image of a PhC slab-on-silicon substrate structure similarly fabricated with the PhC optically characterized below. The inset shows a PhC plane view around the cavity.

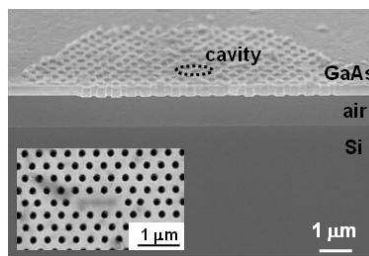


Fig. 2 Cross-sectional scanning electron microscope (SEM) image of the air-bridge structure of InAs/GaAs QD - PhC on silicon substrate. (Inset) Plane view of the PhC structure around the cavity.

## 2.4 Optical characterization

Optical measurements were conducted with a micro-photoluminescence ( $\mu$ -PL) setup at RT using a CW laser diode ( $\lambda = 785$  nm) as the excitation source. The pump laser beam was focused to a 4  $\mu$ m diameter spot on the sample surface by a microscope objective (50x, numerical aperture = 0.42), and was positioned on the PhCs using piezo-electric nanopositioners. The PL emitted from the PhC surface was collected by the same microscope objective.

## 3. Results and discussion

Figure 3(a) shows the lasing PL spectrum from the photonic crystal nanocavity with 100  $\mu$ W CW incident pump light at RT. The sharp peak observed at 1324 nm (= 0.94 eV) corresponds to the light emission from the fundamental cavity mode, the only cavity mode within the range of the ground state energies of the InAs QD ensemble seen in the PL spectrum from the same QD slab but outside the PhC in the inset of Fig. 3(a). The PL intensity ratio of the PhC cavity lasing mode to the background spontaneous emission from the QDs was over 30 dB for pump power above 50  $\mu$ W.

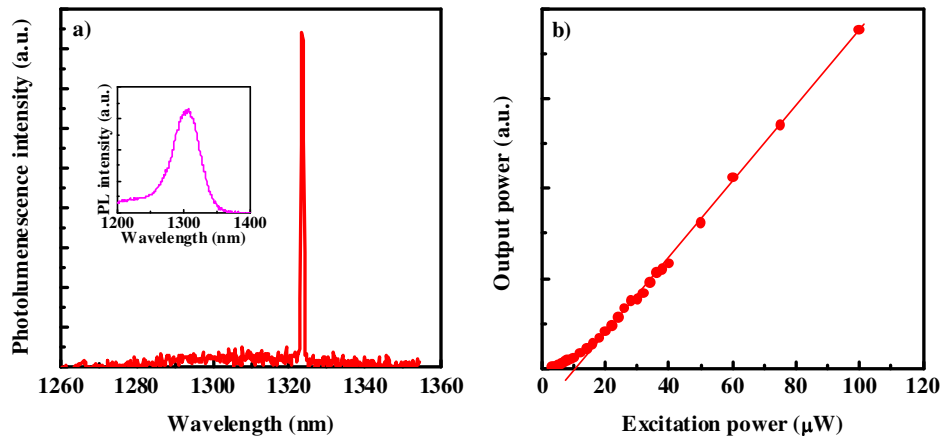


Fig. 3. (a). Photoluminescence spectrum at 100  $\mu$ W incident pump power and (b) output optical power dependence on pump power for the lasing photonic crystal nanocavity mode under continuous-wave optical pumping at room temperature. Also shown in the inset of (a) is a photoluminescence spectrum at 30  $\mu$ W incident pump power for a region of the same InAs/GaAs quantum dot slab but outside the photonic crystal pattern.

Figure 3(b) shows the output optical power dependence on incident pump power (L-L plot) of the lasing mode under CW pumping at RT. The lasing threshold is estimated to be  $\sim 10$   $\mu$ W incident power from these L-L curves and the  $Q$ -factor was  $\sim 8000$  just below the threshold pump power. Such a soft turn-on without apparent kink for lasing onset in the L-L curve is a characteristic of nanocavity lasers with high  $\beta$ -factors [11, 13, 14]. The  $\beta$ -factor is the fraction of the spontaneous emission rate into the lasing mode out of the total spontaneous emission rate and therefore a measure of the optical efficiency of a laser. We will evaluate the  $\beta$ -factor for our device in a following section.

Figure 4 shows the logarithmic L-L plot of the lasing mode under CW pumping at RT, equivalent to the linear L-L plot in Fig. 3(a), and the linewidth dependence on incident pump power. The output power increases linearly with pump power both in the spontaneous and stimulated emission-dominating regions binding a nonlinear slope attributed to lasing onset in

the transition region, around the lasing threshold of 10  $\mu\text{W}$ . The lasing cavity mode linewidth showed a monotonic decrease on pump power following the Schawlow-Townes relation with a partial gradual slope around at 10  $\mu\text{W}$  or the lasing threshold due to phase transition into lasing. Both of these behaviors for the output power and linewidth are consistent with previous experimental [12, 14, 26] and theoretical [26-28] investigations. These results are strong evidences for lasing action in our sample.

In order to determine the  $\beta$ -factor for our PhC nanocavity laser, the experimental L-L plot is compared with theoretical L-L curves calculated using rate equations. A conventional coupled rate model [12, 13, 26] for the carrier density  $N$  and the photon density  $P$  in the nanocavity was used:

$$\frac{dN}{dt} = R_{\text{ex}} - \frac{N}{\tau_r} - \frac{N}{\tau_{nr}} - \frac{c}{n_{\text{eff}}} \cdot \Gamma g(N)P, \quad (1)$$

$$\frac{dP}{dt} = \frac{c}{n_{\text{eff}}} \cdot \Gamma g(N)P + \beta \frac{N}{\tau_r} - \frac{P}{\tau_p}, \quad (2)$$

where  $R_{\text{ex}}$  is the pumping rate,  $\tau_r$  and  $\tau_{nr}$  are the radiative and nonradiative carrier recombination times, respectively, and  $c/n_{\text{eff}} = 1 \times 10^{10}$  cm/s. The confinement factor  $\Gamma$  is estimated as  $\sim 0.006$  from the spacial fraction of the QDs in the slab estimated as  $\sim 0.008$  through transmission electron microscopy (TEM) and atomic force microscopy (AFM) observation for the QDs. The confinement factor in the slab along the growth direction estimated as  $\sim 0.8$  from the calculated field profile across the slab. We assumed a linear gain function  $g(N) = a(N - N_{\text{tr}})$  valid for  $N/N_{\text{tr}} \sim 1$ , which is the case for the range in the L-L plot in Fig. 4, where  $a$  and  $N_{\text{tr}}$  are the differential gain and the transparent carrier density, respectively. We estimate  $a \sim 4 \times 10^{-11}$  cm<sup>2</sup> so that  $\Gamma g(N)$  is equal to the cavity loss  $\sim 20$  cm<sup>-1</sup> estimated from  $Q \sim 8000$  at the threshold pump power. The photon lifetime  $\tau_p$  was estimated to be 5 ps from  $Q \sim 8000$ . Steady state solutions were found and the best fit was obtained with  $N_{\text{tr}} = 4 \times 10^{14}$  cm<sup>-3</sup>,  $\tau_r = 100$  ps and  $\tau_{nr} = 100$  ps. This  $\tau_{nr}$  value is comparable to that of previous studies, in which  $\tau_{nr}$  was estimated through RT time-resolved PL measurement [12, 13]. The  $\tau_r$  value is also reasonable accounting for the  $\tau_r$  measured as  $\sim 1$  ns for QDs located outside of the cavity mode region in Ref. 12 enhanced in the PhC nanocavity by a Purcell factor of  $\sim 10$ , which is consistent with those derived in previous studies using similar QD-PhC systems [13, 29]. The solid red curve in Fig. 4 is the best fit with  $\beta = 0.8$ . However, we carefully claim that  $\beta$  is of the order of 0.1 for our device accounting for the strong dependence of  $\beta$  on other parameters such as  $a$ ,  $N_{\text{tr}}$ ,  $\tau_r$  and  $\tau_{nr}$ . This  $\beta$  value is however still significantly higher than those for conventional QW lasers without PhC.

The effective lasing threshold for our device is estimated at  $\sim 2$   $\mu\text{W}$  by considering the pump light absorbance in the InAs/GaAs QD slab [12]. This value is the lowest among lasers on silicon to the best of our knowledge. Generally lasers with QD gain have significantly lower lasing threshold than QW lasers due to the higher spatial carrier confinement and discrete energy levels in QDs as long as the  $Q$ -factors are large enough to compensate QDs' smaller modal gain than QWs' [9]. As an example, we recently observed a difference of three orders of magnitude between the threshold power of QD- and QW-PhC bandedge lasers with similar PhC structures at 6 K [16]. The effective lasing threshold in this work is still higher than the value of 375 nW of our previously reported QD-PhC nanocavity laser on GaAs substrate with a  $Q$ -factor of  $\sim 90000$  [13], due to the lower  $Q$ -factor of the present device. Optimization of the fabrication process and device design should improve the  $Q$ -factor, and thereby decrease the lasing threshold of the QD-PhC nanocavity lasers on silicon.

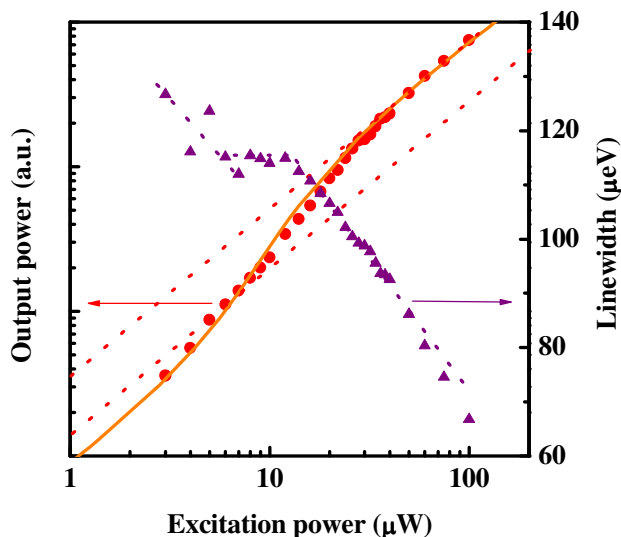


Fig. 4. Logarithmic L-L plot of the lasing photonic crystal nanocavity mode under continuous-wave pumping at room temperature. Also plotted is the linewidth dependence on pump power. The dotted lines fitted to the L-L plot are both linear and the solid curve is a fit by the coupled rate model calculation. The dotted lines fitted to the linewidth plot represent the slope at each region.

#### 4. Summary

In this paper, we report the fabrication of the first QD-PhC nanocavity lasers on silicon. The gain material was InAs/GaAs QDs and this optically-pumped device exhibited CW lasing at RT. This is the first demonstration of RT CW lasing in PhC nanocavities on silicon. The effective lasing threshold was  $\sim 2 \mu\text{W}$ , the lowest for monolithic laser-on-silicon devices ever reported. The on-silicon PhC nanocavity laser structure fabricated in this work could be a basis for highly integrated optical circuits with built-in nanolasers alternative to conventional laborious lateral laser-waveguide interconnections.

#### Acknowledgments

The authors would like to thank Satomi Ishida and Masao Nishioka for their technical support. This work was supported by the Special Coordination Funds for Promoting Science and Technology, the Ministry of Education, Culture, Sports Science and Technology, Japan.